11
Multicolor QCD

The method of $1/N$-expansion can be applied to QCD. This was done by 't Hooft [Hoo74a] using the inverse number of colors for the gauge group $SU(N)$ as an expansion parameter.

For an $SU(N)$ gauge theory without virtual quark loops, the expansion goes in $1/N^2$ and rearranges diagrams of perturbation theory according to their topology. The leading order in $1/N^2$ is given by planar diagrams, which have the topology of a sphere, while the expansion in $1/N^2$ plays the role of a topological expansion. This is similar to an expansion in the string coupling constant in string models of the strong interaction, which also has a topological character.

Virtual quark loops can be easily incorporated in the $1/N$-expansion. One distinguishes between the 't Hooft limit when the number of quark flavors N_{f} is fixed as $N \to \infty$ and the Veneziano limit [Ven76] when the ratio N_{f}/N is fixed as $N \to \infty$. Virtual quark loops are suppressed in the 't Hooft limit as $1/N$ and lead in the Veneziano limit to the same topological expansion as dual-resonance models of strong interaction.

The simplification of QCD in the large-N limit arises from the fact that the number of planar graphs grows with the number of vertices only exponentially rather than factorially as do the total number of graphs. Correlators of gauge-invariant operators factorize in the large-N limit, which looks like the leading-order term of a "semiclassical" WKB-expansion in $1/N$.

We begin this chapter with a description of the double-line representation of diagrams of QCD perturbation theory and rearrange it as the topological expansion in $1/N$. Then we discuss some properties of the $1/N$-expansion for a generic matrix-valued field.

https://doi.org/10.1017/9781009402095.012 Published online by Cambridge University Press

11.1 Index or ribbon graphs

In order to describe the $1/N$-expansion of QCD, the extension of which to N colors has already been considered in Sect. 5.1, it is convenient to use the matrix-field representation (5.5).

In this chapter we shall use a slightly different definition

$$[A_\mu(x)]^{ij} \;=\; \sum_a A^a_\mu(x)\,[t^a]^{ij}\,, \tag{11.1}$$

which is similar to that used by 't Hooft [Hoo74a] and differs from (5.5) by a factor of g:

$$\mathcal{A}^{ij}_\mu(x) \;=\; gA^{ij}_\mu(x)\,. \tag{11.2}$$

The matrix (11.1) is Hermitian.

The propagator of the matrix field $A^{ij}(x)$, in this notation, takes the form

$$\Big\langle A^{ij}_\mu(x)\,A^{kl}_\nu(y)\Big\rangle_{\text{Gauss}} \;=\; \left(\delta^{il}\delta^{kj}-\frac{1}{N}\delta^{ij}\delta^{kl}\right)D_{\mu\nu}(x-y)\,, \tag{11.3}$$

where we have assumed, as usual, a gauge-fixing to define the gluon propagator in perturbation theory. For instance, one has

$$D_{\mu\nu}(x-y) \;=\; \frac{1}{4\pi^2}\frac{\delta_{\mu\nu}}{(x-y)^2} \tag{11.4}$$

in the Feynman gauge.

Equation (11.3) can be derived immediately from the standard formula

$$\Big\langle A^a_\mu(x)\,A^b_\nu(y)\Big\rangle_{\text{Gauss}} \;=\; \delta^{ab}D_{\mu\nu}(x-y) \tag{11.5}$$

multiplying by the generators of the $SU(N)$ gauge group according to the definition (5.5) and using the completeness condition

$$\sum_{a=1}^{N^2-1}(t^a)^{ij}\,(t^a)^{kl} \;=\; \left(\delta^{il}\delta^{kj}-\frac{1}{N}\delta^{ij}\delta^{kl}\right) \qquad \boxed{\text{for}\;\; SU(N)}\,. \tag{11.6}$$

We shall explain in Sect. 13.1 how Eq. (11.3) can be derived directly from a path integral over matrices.

We concentrate in this chapter only on the structure of diagrams in the index space, i.e. the space of the indices associated with the $SU(N)$ group. We shall not consider, in most cases, space-time structures of diagrams which are prescribed by Feynman's rules.

https://doi.org/10.1017/9781009402095.012 Published online by Cambridge University Press

Omitting at large N the second term in parentheses on the RHS of Eq. (11.3), we depict the propagator by the double line

$$\left\langle A_\mu^{ij}(x)\, A_\nu^{kl}(y)\right\rangle_{\text{Gauss}} \;\propto\; \delta^{il}\delta^{kj} \;=\; \begin{array}{l} i \\ j \end{array} \!\!\rightleftarrows\!\! \begin{array}{l} l \\ k \end{array} \quad . \tag{11.7}$$

Each line, often termed the *index line*, represents the Kronecker delta-symbol and has an orientation which is indicated by arrows. This notation is obviously consistent with the space-time structure of the propagator that describes a propagation from x to y.

The arrows are a result of the fact that the matrix A_μ^{ij} is Hermitian and its off-diagonal components are complex conjugate. The independent fields are, say, the complex fields A_μ^{ij} for $i > j$ and the diagonal real fields A_μ^{ii}. The arrow represents the direction of the propagation of the indices of the complex field A_μ^{ij} for $i > j$, while the complex-conjugate field, $A_\mu^{ji} = (A_\mu^{ij})^*$, propagates in the opposite direction. For the real fields A_μ^{ii}, the arrows are not essential.

The double-line notation (11.7) looks similar to that of Sect. 6.5. The reason for that is deep: double lines appear generically in all models describing *matrix* fields in contrast to *vector* (in internal symmetry space) fields, the propagators of which are depicted by single lines as in the previous chapter.

The three-gluon vertex, which is generated by the action (5.13), is depicted in the double-line notation as

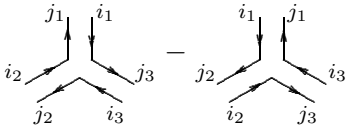

$$\propto\; g\left(\delta^{i_1 j_3}\delta^{i_2 j_1}\delta^{i_3 j_2} - \delta^{i_1 j_2}\delta^{i_2 j_3}\delta^{i_3 j_1}\right), \tag{11.8}$$

where the subscripts 1, 2 or 3 refer to each of the three gluons. The relative minus sign arises from the commutator in the cubic-in-A term in the action (5.13). The color part of the three-vertex is antisymmetric under an interchange of gluons. The space-time structure, which is given in the momentum space as

$$\begin{aligned} &\gamma_{\mu_1\mu_2\mu_3}(p_1, p_2, p_3) \\ &\quad = \;\; \delta_{\mu_1\mu_2}\,(p_1 - p_2)_{\mu_3} + \delta_{\mu_2\mu_3}\,(p_2 - p_3)_{\mu_1} + \delta_{\mu_1\mu_3}\,(p_3 - p_1)_{\mu_2}\ , \end{aligned} \tag{11.9}$$

is antisymmetric as well. We consider all three gluons as incoming so that their momenta obey $p_1 + p_2 + p_3 = 0$. The full vertex is symmetric as prescribed by Bose statistics.

https://doi.org/10.1017/9781009402095.012 Published online by Cambridge University Press

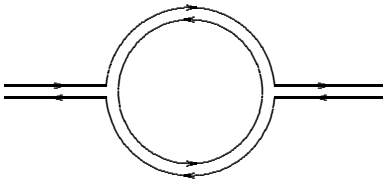

Fig. 11.1. Double-line representation of a one-loop diagram for the gluon propagator. The sum over the N indices is associated with the closed index line. The contribution of this diagram is $\sim g^2 N \sim 1$.

The color structure in Eq. (11.8) can alternatively be obtained by multiplying the standard vertex

$$\Gamma^{a_1 a_2 a_3}_{\mu_1 \mu_2 \mu_3}(p_1, p_2, p_3) \;=\; f^{a_1 a_2 a_3} \gamma_{\mu_1 \mu_2 \mu_3}(p_1, p_2, p_3) \tag{11.10}$$

by $(t^{a_1})^{i_1 j_1} (t^{a_2})^{i_2 j_2} (t^{a_3})^{i_3 j_3}$, with f^{abc} being the structure constants of the $SU(N)$ group, and using the formula

$$f^{a_1 a_2 a_3} (t^{a_1})^{i_1 j_1} (t^{a_2})^{i_2 j_2} (t^{a_3})^{i_3 j_3} \;=\; \mathrm{i} \left(\delta^{i_1 j_3} \delta^{i_2 j_1} \delta^{i_3 j_2} - \delta^{i_1 j_2} \delta^{i_2 j_3} \delta^{i_3 j_1} \right), \tag{11.11}$$

which is a consequence of the completeness condition (11.6).

The four-gluon vertex involves six terms – each of them is depicted by a cross – which differ by interchanging of the color indices. We depict the color structure of the four-gluon vertex for simplicity in the case when $i_1 = j_2 = i$, $i_2 = j_3 = j$, $i_3 = j_4 = k$, $i_4 = j_1 = l$, but i, j, k, l take on different values. Then only the following term is left:

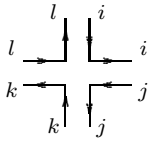

$$\propto\; g^2 \,, \tag{11.12}$$

and there are no delta-symbols on the RHS since the color structure is fixed. In other words, we pick up only one color structure by equating indices pairwise.

The diagrams of perturbation theory can now be completely rewritten in the double-line notation [Hoo74a]. The simplest one which describes the one-loop correction to the gluon propagator is depicted in Fig. 11.1. This diagram involves two three-gluon vertices and a sum over the N indices which is associated with the closed index line analogous to Eq. (6.70). Therefore, the contribution of this diagram is $\sim g^2 N$.

https://doi.org/10.1017/9781009402095.012 Published online by Cambridge University Press

In order for the large-N limit to be nontrivial, the bare coupling constant g^2 should satisfy

$$g^2 \sim \frac{1}{N}. \tag{11.13}$$

This dependence on N is similar to Eqs. (10.14) and (10.65) for the vector models and is prescribed by the asymptotic-freedom formula

$$g^2 = \frac{12\pi^2}{11N \ln(\Lambda/\Lambda_{\rm QCD})} \tag{11.14}$$

of the pure $SU(N)$ gauge theory.

Thus, the contribution of the diagram in Fig. 11.1 is of order

$$\text{Fig. 11.1} \sim g^2 N \sim 1 \tag{11.15}$$

in the large-N limit.

The double lines of the diagram in Fig. 11.1 can be viewed as bounding a piece of a plane. Therefore, these lines represent a two-dimensional object rather than a one-dimensional one as the single lines do in vector models. In mathematics these double-line graphs are often called *ribbon* graphs or *fatgraphs*. In the following we shall see their connection with Riemann surfaces.

Remark on the $U(N)$ gauge group

As was mentioned previously, the second term in the parentheses on the RHS of Eq. (11.6) can be omitted at large N. Such a completeness condition emerges for the $U(N)$ group, the generators of which, T^A $(A = 1, \ldots, N^2)$, are

$$T^A = \left(t^a, \mathbb{I}/\sqrt{N}\right), \qquad \operatorname{tr} T^A T^B = \delta^{AB}. \tag{11.16}$$

They obey the completeness condition

$$\sum_{A=1}^{N^2} \left(T^A\right)^{ij} \left(T^A\right)^{kl} = \delta^{il}\delta^{kj} \qquad \boxed{\text{for } U(N)}. \tag{11.17}$$

The point is that elements of both the $SU(N)$ group and the $U(N)$ group can be represented in the form

$$U = \mathrm{e}^{\mathrm{i}B}, \tag{11.18}$$

where B is a general Hermitian matrix for $U(N)$ and a traceless Hermitian matrix for $SU(N)$.

Therefore, the double-line representation of the perturbation-theory diagrams which is described in this chapter holds, strictly speaking, only for the $U(N)$ gauge group. However, the large-N limit of both the $U(N)$ group and the $SU(N)$ group is the same.

https://doi.org/10.1017/9781009402095.012 Published online by Cambridge University Press

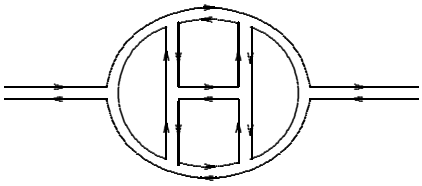

Fig. 11.2. Double-line representation of a four-loop diagram for the gluon propagator. The sum over the N indices is associated with each of the four closed index lines, the number of which is equal to the number of loops. The contribution of this diagram is $\sim g^8 N^4 \sim 1$.

11.2 Planar and nonplanar graphs

The double-line representation of perturbation-theory diagrams in the index space is very convenient to estimate their orders in $1/N$. Each three- or four-gluon vertex contributes a factor of g or g^2, respectively. Each closed index line contributes a factor of N. The order of g in $1/N$ is given by Eq. (11.13).

Let us consider a typical diagram for the gluon propagator depicted in Fig. 11.2. It has eight three-gluon vertices and four closed index lines, which coincides with the number of loops. Therefore, the order of this diagram in $1/N$ is

$$\text{Fig. 11.2} \;\sim\; \left(g^2 N\right)^4 \;\sim\; 1\,. \tag{11.19}$$

The diagrams of the type in Fig. 11.2, which can be drawn on a sheet of paper without crossing any lines, are called *planar* diagrams. For such diagrams, the addition of a loop inevitably results in the addition of two three-gluon (or one four-gluon) vertices. A planar diagram with n_2 loops has n_2 closed index lines. It is of order

$$n_2\text{-loop planar diagram} \;\sim\; \left(g^2 N\right)^{n_2} \;\sim\; 1\,, \tag{11.20}$$

so that all planar diagrams survive in the large-N limit.

Let us now consider a *nonplanar* diagram of the type depicted in Fig. 11.3. This diagram is a three-loop one and has six three-gluon vertices. The crossing of the two lines in the middle does not correspond to a four-gluon vertex and is merely a result of the fact that the diagram cannot be drawn on a sheet of paper without crossing the lines. The diagram has only one closed index line. The order of this diagram in $1/N$ is

$$\text{Fig. 11.3} \;\sim\; g^6 N \;\sim\; \frac{1}{N^2}\,. \tag{11.21}$$

It is therefore suppressed at large N by $1/N^2$.

https://doi.org/10.1017/9781009402095.012 Published online by Cambridge University Press

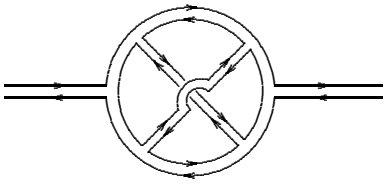

Fig. 11.3. Double-line representation of a three-loop nonplanar diagram for the gluon propagator. The diagram has six three-gluon vertices but only one closed index line (although it has three loops!). The order of this diagram is $\sim g^6 N \sim 1/N^2$.

The nonplanar diagram in Fig. 11.3 can be drawn without line-crossing on a surface with one handle which in mathematics is usually called a torus or a surface of genus one. A plane is then equivalent to a sphere and has genus zero. Adding a handle to a surface produces a hole according to mathematical terminology. A general Riemann surface with h holes has genus h.

The above evaluations of the order of the diagrams in Figs. 11.1–11.3 can be described by the single formula

$$\text{genus-}h \text{ diagram } \sim \left(\frac{1}{N^2}\right)^{\text{genus}} . \tag{11.22}$$

Thus, the expansion in $1/N$ rearranges perturbation-theory diagrams according to their topology [Hoo74a]. For this reason, it is referred to as the *topological expansion* or the *genus expansion*. The general proof of Eq. (11.22) for an arbitrary diagram is given in Sect. 11.4.

Only planar diagrams, which are associated with genus zero, survive in the large-N limit. This class of diagrams is an analog of the bubble graphs in the vector models. However, the problem of summing the planar graphs is much more complicated than that of summing the bubble graphs. Nevertheless, it is simpler than the problem of summing all the graphs, since the number of planar graphs with n_0 vertices grows geometrically at large n_0 [Tut62, KNN77]

$$\#_{\rm p}(n_0) \equiv \text{ no of planar graphs } \sim \text{ const}^{n_0} , \tag{11.23}$$

while the total number of graphs grows factorially with n_0. There is no dependence in Eq. (11.23) on the number of external lines of a planar graph which is assumed to be much less than n_0.

It is instructive to see the difference between the planar diagrams and, for instance, the ladder diagrams which describe e^+e^- elastic scattering in QED. Let the ladder have n rungs. Then there are $n!$ ladder diagrams, but

https://doi.org/10.1017/9781009402095.012 Published online by Cambridge University Press

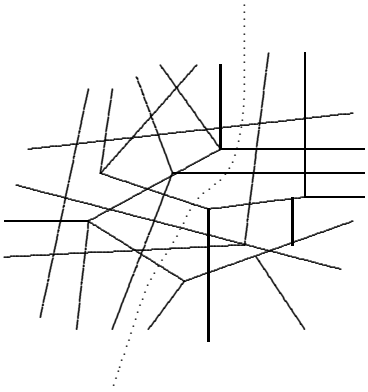

Fig. 11.4. Cutting a planar graph into two graphs. The cutting is along the dotted line. The numbers of vertices of each part and of the whole graph obey Eq. (11.24).

only one of them is planar. This simple example shows why the number of planar graphs is much smaller than the total number of graphs, most of which are nonplanar.

In the rest of this book, we shall discuss what is known concerning solving the problem of summing the planar graphs.

Problem 11.1 Show that Eq. (11.23) for the number of planar graphs is consistent with its independence of the number of external lines.

Solution Let us split a planar graph into two parts by cutting along some line as depicted in Fig. 11.4. The numbers of vertices of each part, n_0' and n_0'', are obviously related to that of the original graph, n_0, by

$$n_0' + n_0'' \;=\; n_0\,. \tag{11.24}$$

We assume that both n_0' and n_0'' are large.

The number of cut lines is $\sim \sqrt{n_0}$ for a planar graph in contrast to that for a generic nonplanar one, when it would be $\sim n_0$. Disregarding the cut lines, we obtain

$$\#_{\rm p}(n_0) \;=\; \#_{\rm p}(n_0')\cdot\#_{\rm p}(n_0'')\,, \tag{11.25}$$

which is obviously satisfied by the formula (11.23) accounting for Eq. (11.24).

Problem 11.2 Cutting all loops of a planar graph, obtain the upper bound

$$\#_{\rm p} \;\le\; (1024)^{n_2} \tag{11.26}$$

for the number of planar graphs with n_2 loops.

Solution Since $\#_{\rm p}$ does not depend on the number of external lines (see Problem 11.1), let us consider a one-particle irreducible planar graph with one external line and cut all the loops as depicted in Fig. 11.5a. By a continuous

https://doi.org/10.1017/9781009402095.012 Published online by Cambridge University Press

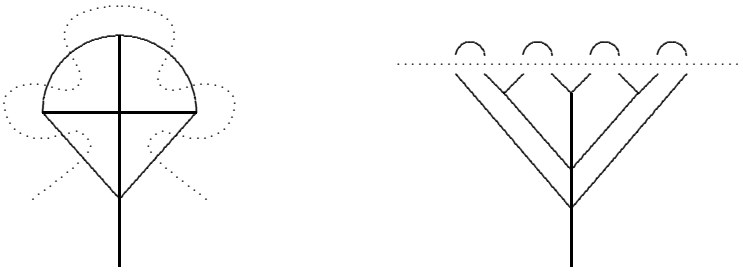

(a) (b)

Fig. 11.5. Cutting a planar graph into trees and arches. The line of cutting is depicted in (a) by a dotted line. The combination of tree and arches in (b) is obtained from (a) by a continuous distortion.

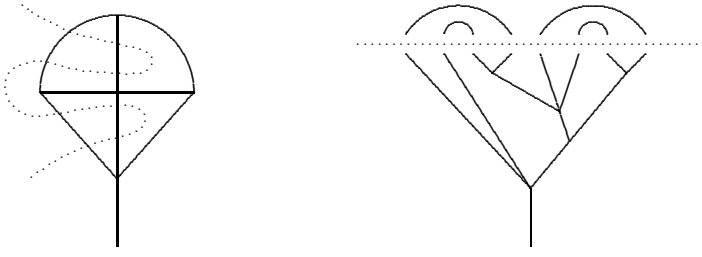

(a) (b)

Fig. 11.6. Alternative cutting of the same planar graph as in Fig. 11.5 into trees and arches.

distortion, it can be depicted as in Fig. 11.5b, where below the dotted line we have a tree with n_0 vertices and above the dotted line we have n_2 arches. The latter number coincides with the number of loops of the planar graph. The number of tips of the tree is $2n_2$.

Since each planar graph can be cut in several ways, $\#_{\rm p}$ is bounded from above by

$$\#_{\rm p} \;\leq\; \#_{\rm A}(n_2)\,\#_{\rm T}(n_0, 2n_2)\,, \tag{11.27}$$

where $\#_{\rm A}(n_2)$ denotes the number of arches and $\#_{\rm T}(n_0, 2n_2)$ denotes the number of trees with n_0 vertices and $2n_2$ tips. An alternative way of cutting the same planar graph, which leads to a different combination of arches and trees, is depicted in Fig. 11.6.

https://doi.org/10.1017/9781009402095.012 Published online by Cambridge University Press

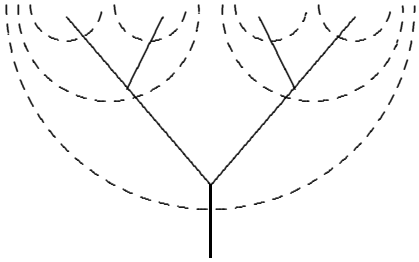

Fig. 11.7. A tree graph (the solid lines) and its dual (the dashed arches).

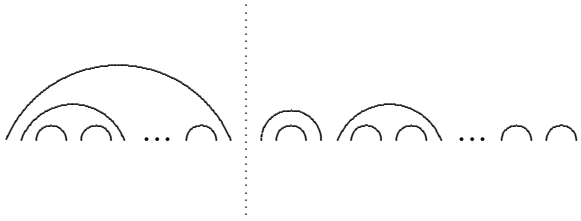

Fig. 11.8. Recurrence relation for the number of arches. The dotted line separates a configuration of n arches into two pieces: n' to the left and $n - n'$ to the right.

The number of arches is well-known in mathematics and is given by the Catalan number of order n:

$$\#_{\rm A}(n) \;=\; \frac{2n!}{n!(n+1)!} \;\stackrel{n\to\infty}{\longrightarrow}\; 4^n\,. \tag{11.28}$$

The number of trees is not independent since a graph, dual to a tree graph, consists of arches as is illustrated by Fig. 11.7. The number of arches of this dual graph equals the sum of the number n_0 of vertices and the number $2n_2$ of tips, i.e. equals $n_0 + 2n_2$. Given the number n_2 of loops, the number n_0 of vertices is maximal when all vertices are trivalent, so that

$$n_0 \;\le\; 2n_2 - 1 \tag{11.29}$$

($n_0 = 2n_2$ for trivalent and $n_0 = n_2$ for fourvalent vertices when n_2 is large). Therefore, the number of arches of the dual graph is bounded by $4n_2$, so that

$$\#_{\rm T}(n_0, 2n_2) \;\le\; \#_{\rm A}(4n_2)\,. \tag{11.30}$$

Substituting in (11.27), we obtain [KNN77] the inequality (11.26).

Finally, Eq. (11.23) can be obtained by noting that $n_0 \sim n_2$ for large n_2.

Problem 11.3 Derive Eq. (11.28) for the number of arches.

Solution Let us consider a general configuration of n arches as depicted in Fig. 11.8. Let us pick up the leftmost arch, splitting the configuration into two

https://doi.org/10.1017/9781009402095.012 Published online by Cambridge University Press

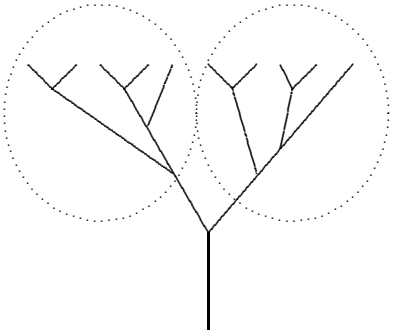

Fig. 11.9. Recurrence relation for the number of trees. The trees inside the left and right dotted circles have n' and $n-n'$ tips, respectively.

pieces: n' arches to the left and $n-n'$ arches to the right of the dotted line. The number of arches obviously satisfies the recurrence relation

$$\#_{\rm A}(n) \;=\; \sum_{n'=1}^{n} \#_{\rm A}(n'-1)\,\#_{\rm A}(n-n')\,, \tag{11.31}$$

where the number of arches to the left of the dotted line is described by $\#_{\rm A}(n'-1)$ because one arch encircles $n'-1$ others. Equation (11.31) expresses $\#_{\rm A}(n)$ recurrently via $\#_{\rm A}(0)=1$.

Introducing the generating function

$$f_{\rm A}(g) \;=\; \sum_{n=0}^{\infty} g^{n+1}\#_{\rm A}(n)\,, \tag{11.32}$$

we rewrite Eq. (11.31) as the quadratic equation

$$f_{\rm A}(g)-g \;=\; f_{\rm A}^2(g)\,. \tag{11.33}$$

Its solution

$$f_{\rm A}(g) \;=\; \frac{1-\sqrt{1-4g}}{2} = \sum_{n=0}^{\infty} g^{n+1}\frac{(2n)!}{n!(n+1)!} \tag{11.34}$$

gives Eq. (11.28) for the number of arches.

Problem 11.4 Improve the inequality (11.26), calculating the number of trivalent tree graphs with n tips.

Solution Let us first note that the number of vertices of a trivalent tree graph with n tips equals $n-1$. Hence, we are interested in

$$\#_{\rm T}(n) \;\equiv\; \#_{\rm T}(n-1,n) \tag{11.35}$$

in the notation of Problem 11.2. Picking up the first vertex in a tree as depicted in Fig. 11.9, we obtain the following recursion relation for the number of trivalent

https://doi.org/10.1017/9781009402095.012 Published online by Cambridge University Press

tree graphs:

$$\#_{\rm T}(n) \;=\; \sum_{n'=1}^{n-1} \#_{\rm T}(n')\,\#_{\rm T}(n-n')\,, \tag{11.36}$$

which expresses $\#_{\rm T}(n)$ via $\#_{\rm T}(1)=1$.

Introducing the generating function

$$f_{\rm T}(g) \;=\; \sum_{n=1}^{\infty} g^{n-1}\#_{\rm T}(n)\,, \tag{11.37}$$

where g^{n-1} corresponds to $n-1$ vertices of each tree, we rewrite Eq. (11.36) as the quadratic equation

$$f_{\rm T}(g)-1 \;=\; g f_{\rm T}^2(g)\,. \tag{11.38}$$

Its solution

$$f_{\rm T}(g) \;=\; \frac{1-\sqrt{1-4g}}{2g} = \sum_{n=1}^{\infty} g^{n-1}\frac{(2n-2)!}{n!\,(n-1)!} \tag{11.39}$$

gives

$$\#_{\rm T}(n) \;=\; \frac{(2n-2)!}{n!(n-1)!}\,. \tag{11.40}$$

Returning to Problem 11.2, it is shown that

$$\#_{\rm T}(n_0,2n_2) \;\le\; \#_{\rm T}(2n_2-1,2n_2) \;=\; \#_{\rm A}(2n_2-1)\,. \tag{11.41}$$

The inequality here is a result of (11.29) and the equality is because of the explicit formulas (11.28) and (11.40). Thus we have improved the estimate (11.30) having calculated the number of tree graphs. The inequality (11.26) is now improved as

$$\#_{\rm p} \;\le\; (64)^{n_2}\,. \tag{11.42}$$

The actual number of planar graphs was first evaluated by Tutte [Tut62]. In Sect. 13.2 we shall obtain the estimate

$$\#_{\rm p} \;\approx\; \left(12\sqrt{3}\right)^{n_2} \tag{11.43}$$

for the number of trivalent planar graphs at asymptotically large n_2.

11.3 Planar and nonplanar graphs (the boundaries)

Equation (11.22) holds, strictly speaking, only for the gluon propagator, while the contribution of all planar diagrams to a connected n-point Green function is $\sim g^{n-2}$, which is its natural order in $1/N$. The three-gluon Green function is $\sim g$, the four-gluon one is $\sim g^2$ and so on. In order to make contributions of all planar diagrams to be of the same order ~ 1 in the large-N limit, independently of the number of external lines, it is convenient to contract the Kronecker delta-symbols associated with external lines.

https://doi.org/10.1017/9781009402095.012 Published online by Cambridge University Press

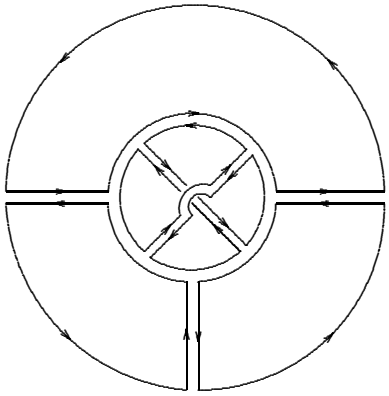

Fig. 11.10. Generic index diagram with $n_0 = 10$ vertices, $n_1 = 10$ gluon propagators, $n_2 = 4$ closed index lines, and $B = 1$ boundary. The color indices of the external lines are contracted by the Kronecker delta-symbols (represented by the single lines) in a cyclic order. The extra factor of $1/N$ arises from the normalization (11.44). Its order in $1/N$ is $\sim 1/N^2$ in accord with Eq. (11.22).

Let us do this in a cyclic order as depicted in Fig. 11.10 for a generic connected diagram with three external gluon lines. The extra delta-symbols, which are added to contract the color indices, are depicted by the single lines. They can be viewed as a *boundary* of the given diagram. The actual size of the boundary is not essential – it can be shrunk to a point. Then a bounded piece of a plane will be topologically equivalent to a sphere with a puncture. I shall prefer to draw planar diagrams in a plane with an extended boundary (boundaries) rather than in a sphere with a puncture (punctures).

It is clear from the graphical representation that the diagram in Fig. 11.10 is associated with the trace over the color indices of the three-point Green function

$$G^{(3)}_{\mu_1\mu_2\mu_3}(x_1, x_2, x_3) \equiv \frac{g^3}{N} \langle \operatorname{tr} [A_{\mu_1}(x_1)\, A_{\mu_2}(x_2)\, A_{\mu_3}(x_3)] \rangle . \qquad (11.44)$$

Here we have introduced the factor of g^3/N to make $G^{(3)}$ of $\mathcal{O}(1)$ in the large-N limit. Therefore, the contribution of the diagram in Fig. 11.10 having one boundary should be divided by N, while the factor of g^3 is naturally associated with three extra vertices which appear after the contraction of color indices.

The extension of Eq. (11.44) to multipoint Green functions is obvious:

$$G^{(n)}_{\mu_1\cdots\mu_n}(x_1, \ldots, x_n) \equiv \frac{g^n}{N} \langle \operatorname{tr} [A_{\mu_1}(x_1) \cdots A_{\mu_n}(x_n)] \rangle . \qquad (11.45)$$

https://doi.org/10.1017/9781009402095.012 Published online by Cambridge University Press

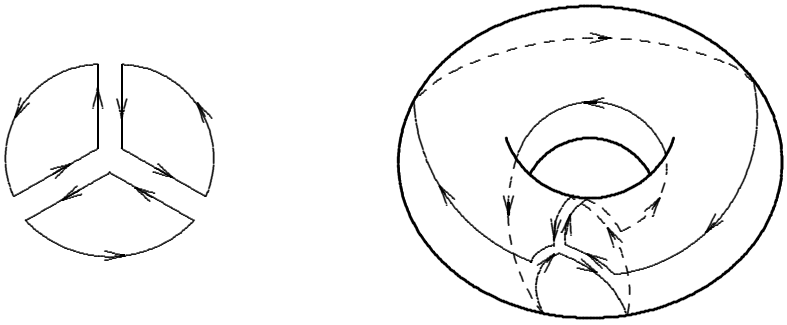

(a) (b)

Fig. 11.11. Planar (a) and nonplanar (b) contributions of the two color structures in Eq. (11.8) for three-gluon vertex to $G^{(3)}$ in the lowest order of perturbation theory.

The factor of $1/N$, which normalizes the trace, provides the natural normalization $G^{(0)} = 1$ of the averages.

Though the two terms in the index-space representation (11.8) of the three-gluon vertex look very similar, their fate in the topological expansion is quite different. When the color indices are contracted anticlockwise, the first term leads to the planar contributions to $G^{(3)}$, the simplest of which is depicted in Fig. 11.11a. The anticlockwise contraction of the color indices in the second term leads to a nonplanar graph in Fig. 11.11b which can be drawn without a crossing of lines only on a torus. Therefore, the two color structures of the three-gluon vertex contribute to different orders of the topological expansion. The same is true for the four-gluon vertex.

Remark on oriented Riemann surfaces

Each line of an index graph of the type depicted in Fig. 11.10 is oriented. This orientation continues along a closed index line, while the pairs of index lines of each double line have opposite orientations. The overall orientation of the lines is prescribed by the orientation of the external boundary which we choose to be, say, anticlockwise. Since the lines are oriented, the faces of the Riemann surface associated with a given graph are also oriented – all in the same way – anticlockwise. Vice versa, such an orientation of the Riemann surfaces unambiguously fixes the orientation of all the index lines. This is the reason why we shall often omit the

(a) (b)

Fig. 11.12. Example of (a) connected and (b) disconnected planar graphs.

arrows associated with the orientation of the index lines: their directions are obvious.

Remark on cyclic-ordered Green functions

The cyclic-ordered Green functions (11.45) arise naturally in the expansion of the trace of the non-Abelian phase factor for a closed contour, which was considered in Problem 5.2 on p. 89. One obtains

$$\left\langle \frac{1}{N} \operatorname{tr} \boldsymbol{P}\, \mathrm{e}^{\mathrm{i}g \oint_\Gamma \mathrm{d}x^\mu A_\mu(x)} \right\rangle = \sum_{n=0}^{\infty} \mathrm{i}^n \oint_\Gamma \mathrm{d}x_1^{\mu_1} \int_{x_1}^{x_1} \mathrm{d}x_2^{\mu_2} \dots \int_{x_1}^{x_{n-1}} \mathrm{d}x_n^{\mu_n}\, G^{(n)}_{\mu_1 \dots \mu_n}(x_1, \dots, x_n)\,. \tag{11.46}$$

The reason for this is that the ordering along a closed path implies cyclic-ordering in the index space.

Remark on generating functionals for planar graphs

By connected or disconnected planar graphs we mean, respectively, the graphs which were connected or disconnected before the contraction of the color indices as illustrated by Fig. 11.12. The graph in Fig. 11.12a is connected-planar, while the graph in Fig. 11.12b is disconnected-planar.

The usual relation (2.52) between the generating functionals $W[J]$ and $Z[J]$ for connected graphs and all graphs, which is discussed in the Remark on p. 44, does not hold for the planar graphs. The reason for this is that exponentiation of such a connected planar diagram for the cyclic-ordered Green functions (11.45) can give disconnected nonplanar diagrams.

https://doi.org/10.1017/9781009402095.012 Published online by Cambridge University Press

The generating functionals for all and connected planar graphs can be constructed [Cvi81] by means of introducing noncommutative sources $\boldsymbol{j}_\mu(x)$. "Noncommutative" means that there is no way to transform $\boldsymbol{j}_{\mu_1}(x_1)\,\boldsymbol{j}_{\mu_2}(x_2)$ into $\boldsymbol{j}_{\mu_2}(x_2)\,\boldsymbol{j}_{\mu_1}(x_1)$. This noncommutativity of the sources reflects the cyclic-ordered structure of the Green functions (11.45) which possess only cyclic symmetry.

Using the shorthand notation (10.62) where the symbol $\circ$ includes the sum over the d-vector (or whatever is available) indices except for the color ones:

$$\boldsymbol{j}\circ\mathcal{A} \;\equiv\; \sum_\mu \int \mathrm{d}^d x\, \boldsymbol{j}_\mu(x)\,\mathcal{A}_\mu(x)\,, \tag{11.47}$$

we write down the definitions of the generating functionals for all planar and connected planar graphs, respectively, as

$$Z[\boldsymbol{j}] \;\equiv\; \sum_{n=0}^{\infty} \mathrm{i}^n \left\langle \frac{1}{N}\,\mathrm{tr}\,(\boldsymbol{j}\circ\mathcal{A})^n \right\rangle \tag{11.48}$$

and

$$W[\boldsymbol{j}] \;\equiv\; \sum_{n=0}^{\infty} \mathrm{i}^n \left\langle \frac{1}{N}\,\mathrm{tr}\,(\boldsymbol{j}\circ\mathcal{A})^n \right\rangle_{\mathrm{conn}}\,. \tag{11.49}$$

The planar contribution to the Green functions (11.45) and their connected counterparts can be obtained, respectively, from the generating functionals $Z[\boldsymbol{j}]$ and $W[\boldsymbol{j}]$ by applying the noncommutative derivative which is defined by

$$\frac{\delta}{\delta \boldsymbol{j}_\mu(x)}\boldsymbol{j}_\nu(y) f(\boldsymbol{j}) \;=\; \delta_{\mu\nu}\,\delta^{(d)}(x-y)\,f(\boldsymbol{j})\,, \tag{11.50}$$

where f is an arbitrary function of $\boldsymbol{j}_\mu$. In other words, the derivative picks up only the leftmost variable.

The relation which replaces Eq. (2.52) for planar graphs is

$$Z[\boldsymbol{j}] \;=\; W[\boldsymbol{j}\,Z[\boldsymbol{j}]]\,, \tag{11.51}$$

while the cyclic symmetry gives

$$W[\boldsymbol{j}\,Z[\boldsymbol{j}]] \;=\; W[Z[\boldsymbol{j}]\,\boldsymbol{j}]\,. \tag{11.52}$$

A graphical derivation of Eqs. (11.51) and (11.52) is given in Fig. 11.13. In other words, given $W[\boldsymbol{j}]$, one should construct an inverse function as the solution to the equation

$$\boldsymbol{j}_\mu(x) \;=\; \boldsymbol{J}_\mu(x)\,W[\boldsymbol{j}]\,, \tag{11.53}$$

https://doi.org/10.1017/9781009402095.012 Published online by Cambridge University Press

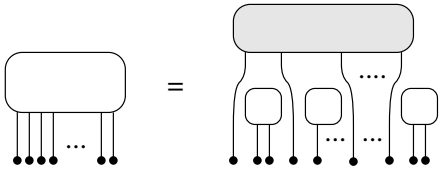

Fig. 11.13. Graphical derivation of Eq. (11.51): $Z[\boldsymbol{j}]$ is denoted by an empty box, $W[\boldsymbol{j}]$ is denoted by a shaded box, $\boldsymbol{j}$ is denoted by a filled circle. By picking the leftmost external line of a planar graph, we end up with a connected planar graph, whose remaining external lines are somewhere to the right interspersed by disconnected planar graphs. It is evident that $\boldsymbol{j}Z[\boldsymbol{j}]$ plays the role of a new source for the connected planar graph. If we instead pick up the rightmost external line, we obtain the inverse order $Z[\boldsymbol{j}]\,\boldsymbol{j}$, which results in Eq. (11.52).

after which Eq. (11.51) gives

$$Z[\boldsymbol{j}] \;=\; W[\boldsymbol{J}]\,. \tag{11.54}$$

More concerning this approach to the generating functionals for planar graphs can be found in [CLS82].

Problem 11.5 Solve Eq. (11.51) iteratively for the Gaussian case.

Solution In the Gaussian case, only $G^{(2)}$ is nonvanishing which yields

$$W[\boldsymbol{j}] \;=\; 1 - g^2 \boldsymbol{j} \circ D \circ \boldsymbol{j}\,, \tag{11.55}$$

where the propagator D is given by Eq. (11.4). Using Eq. (11.51), we find explicitly

$$Z[\boldsymbol{j}] \;=\; 1 - g^2 \int \mathrm{d}^d x\, \mathrm{d}^d y\, D_{\mu\nu}(x-y)\, \boldsymbol{j}_\mu(x)\, Z[\boldsymbol{j}]\, \boldsymbol{j}_\nu(y)\, Z[\boldsymbol{j}]\,. \tag{11.56}$$

While this equation for $Z\,[\boldsymbol{j}]$ is quadratic, its solution can be written only as a continued fraction owing to the noncommutative nature of the variables. In order to find it, we rewrite Eq. (11.56) as

$$Z[\boldsymbol{j}] \;=\; \frac{1}{1 + g^2 \int \mathrm{d}^d x\, \mathrm{d}^d y\, D_{\mu\nu}(x-y)\, \boldsymbol{j}_\mu(x)\, Z[\boldsymbol{j}]\, \boldsymbol{j}_\nu(y)}\,, \tag{11.57}$$

the iterative solution of which is given by [Cvi81]

$$Z[\boldsymbol{j}] \;=\; \cfrac{1}{1 + g^2 \boldsymbol{j} \cfrac{\circ D \circ}{1 + g^2 \boldsymbol{j} \cfrac{\circ D \circ}{1 + g^2 \boldsymbol{j} \cfrac{\circ D \circ}{\boldsymbol{j}}}}}\,. \tag{11.58}$$

https://doi.org/10.1017/9781009402095.012 Published online by Cambridge University Press

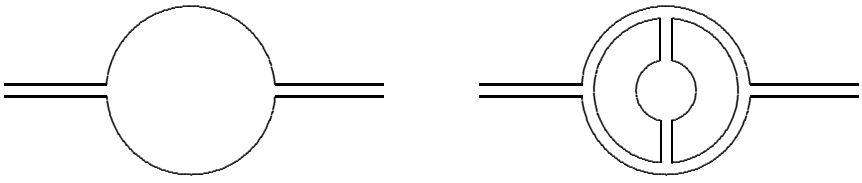

(a) (b)

Fig. 11.14. Diagrams for the gluon propagator with a quark loop which is represented by the single lines. Diagram (a) involves one quark loop and has no closed index lines so that its order is $\sim g^2 \sim 1/N$. Diagram (b) involves three loops, one of which is a quark loop. Its order is $\sim g^6 N^2 \sim 1/N$.

11.4 Topological expansion and quark loops

It is easy to incorporate quarks in the topological expansion. A quark field belongs to the fundamental representation of the gauge group $SU(N)$ and its propagator is represented by a single line

$$\left\langle \psi_i \bar{\psi}_j \right\rangle \;\propto\; \delta_{ij} \;=\; i \longrightarrow j \,. \tag{11.59}$$

The arrow indicates, as usual, the direction of propagation of a (complex) field ψ. We shall omit these arrows for simplicity.

The diagram for the gluon propagator which involves one quark loop is depicted in Fig. 11.14a. It has two three-gluon vertices and no closed index lines so that its order in $1/N$ is

$$\text{Fig. 11.14a} \;\sim\; g^2 \;\sim\; \frac{1}{N} \,. \tag{11.60}$$

Analogously, the order of a more complicated tree-loop diagram in Fig. 11.14b, which involves one quark loop and two closed index lines, is

$$\text{Fig. 11.14b} \;\sim\; g^6 N^2 \;\sim\; \frac{1}{N} \,. \tag{11.61}$$

It is evident from this consideration that quark loops are not accompanied by closed index lines. One should add a closed index line for each quark loop in order for a given diagram with L quark loops to have the same double-line representation as for pure gluon diagrams. Therefore, given Eq. (11.22), diagrams with L quark loops are suppressed at large N by

$$L \text{ quark loops} \;\sim\; \left(\frac{1}{N}\right)^{L+2\cdot\text{genus}} \,. \tag{11.62}$$

https://doi.org/10.1017/9781009402095.012 Published online by Cambridge University Press

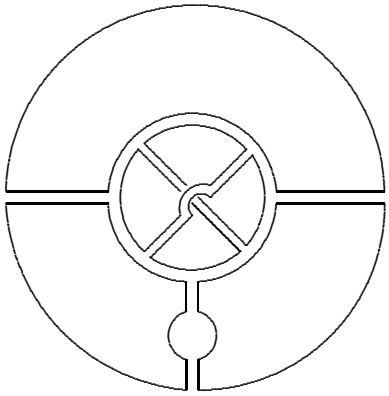

Fig. 11.15. Generic diagram in the index space which has $L = 1$ quark loop and $B = 1$ loop associated with the external boundary. Its order in $1/N$ is described by Eq. (11.70).

The single-line representation of the quark loops is similar to that of the external boundary in Fig. 11.10. Moreover, such a diagram emerges when one calculates perturbative gluon corrections to the vacuum expectation value of the quark operator

$$O \;=\; \frac{1}{N}\bar{\psi}\psi\,, \tag{11.63}$$

where the factor of $1/N$ is introduced to make it $\mathcal{O}(1)$ in the large-N limit. Therefore, the external boundary can be viewed as a single line associated with valence quarks. The difference between virtual quark loops and external boundaries is that each of the latter has a factor of $1/N$ owing to the definitions (11.45) and (11.63).

In order to prove Eqs. (11.22) and its quark counterpart (11.62), let us consider a generic diagram in the index space which has $n_0^{(3)}$ three-point vertices (either three-gluon or quark–gluon ones), $n_0^{(4)}$ four-gluon vertices, n_1 propagators (either gluon or quark ones), n_2 closed index lines, L virtual quark loops and B external boundaries. A typical such diagram is depicted in Fig. 11.15. Its order in $1/N$ is

$$\frac{1}{N^B} g^{n_0^{(3)}+2n_0^{(4)}} N^{n_2} \quad\sim\quad N^{n_2-n_0^{(3)}/2-n_0^{(4)}-B} \tag{11.64}$$

as has already been explained. The extra factor of $1/N^B$ arises from the extra normalization factor of $1/N$ in operators associated with external boundaries.

The number of propagators and vertices are related by

$$2n_1 \;=\; 3n_0^{(3)} + 4n_0^{(4)}, \tag{11.65}$$

https://doi.org/10.1017/9781009402095.012 Published online by Cambridge University Press

since three- and four-point vertices emit three or four propagators, respectively, and each propagator connects two vertices. Using the relation (11.65), we rewrite the RHS of (11.64) as

$$N^{n_2-n_0^{(3)}/2-n_0^{(4)}-B} \;=\; N^{n_2-n_1+n_0-B}, \tag{11.66}$$

where the total number of vertices

$$n_0 \;=\; n_0^{(3)} + n_0^{(4)} \tag{11.67}$$

is introduced.

The exponent on the RHS of Eq. (11.66) can be expressed via the Euler characteristic χ of a given graph of genus h. Let us first mention that an appropriate Riemann surface, which is associated with a given graph, is open and has $B+L$ boundaries (represented by single lines). This surface can be closed by attaching a cap to each boundary. The single lines then become double-lines together with the lines of the boundary of each cap. We have already considered this procedure when deducing Eq. (11.62) from Eq. (11.22).

The number of faces for a closed Riemann surface constructed in such a manner is $n_2 + L + B$, while the number of edges and vertices are n_1 and n_0, respectively. Euler's theorem states that

$$\chi \;\equiv\; 2-2h \;=\; n_2 + L + B - n_1 + n_0\,. \tag{11.68}$$

Therefore the RHS of Eq. (11.66) can be rewritten as

$$N^{n_2-n_1+n_0-B} \;=\; N^{2-2h-L-2B}. \tag{11.69}$$

We have thus proven that the order in $1/N$ of a generic graph does not depend on its order in the coupling constant and is completely expressed via the genus h and the number of virtual quark loops L and external boundaries B by

$$\text{generic graph} \;\sim\; \left(\frac{1}{N}\right)^{2h+L+2(B-1)}. \tag{11.70}$$

For $B=1$, we recover Eqs. (11.22) and (11.62).

Remark on the order of gauge action

We see from Eq. (11.45) that the natural variables for the large-N limit are the calligraphic matrices $\mathcal{A}_\mu$ which include the extra factor of g with respect to A_μ (see Eq. (11.2)). For these matrices

$$\frac{1}{N}\,\langle\,\mathrm{tr}\,[\mathcal{A}_{\mu_1}(x_1)\cdots\mathcal{A}_{\mu_n}(x_n)]\,\rangle \;=\; G^{(n)}_{\mu_1\cdots\mu_n}(x_1,\ldots,x_n) \tag{11.71}$$

so that they are $\mathcal{O}(1)$ in the large-N limit since the trace is $\mathcal{O}(N)$.

https://doi.org/10.1017/9781009402095.012 Published online by Cambridge University Press

In these variables, the gluon part of the QCD action (5.13) takes the simple form

$$S \;=\; \frac{1}{4g^2}\int \mathrm{d}^d x\, \mathrm{tr}\, \mathcal{F}_{\mu\nu}^2(x)\,. \tag{11.72}$$

Since g^2 in this formula is $\sim 1/N$ and the trace is $\sim N$, the action is $\mathcal{O}\big(N^2\big)$ at large N.

This result can be anticipated from the free theory because the kinetic part of the action involves the sum over N^2-1 free gluons. Therefore, the non-Abelian field strength (3.62) is ~ 1 for $g^2 \sim 1/N$.

The fact that the action is $\mathcal{O}\big(N^2\big)$ in the large-N limit is a generic property of the models describing matrix fields. It will be crucial for developing saddle-point approaches at large N which are considered below.

Problem 11.6 Rederive the formula (11.70) using the calligraphic notation.

Solution The propagator of the $\mathcal{A}$-field is $\sim g^2$, while both three- and four-gluon vertices are now $\sim g^{-2}$ as a consequence of Eq. (11.72). The contribution of a generic graph is now of the order

$$\big(g^2\big)^{n_1-n_0}\, N^{n_2-B} \;\;\sim\;\; N^{n_2-n_1+n_0-B} \tag{11.73}$$

for $g^2 \sim 1/N$. This coincides with the RHS of Eq. (11.66) which results in Eq. (11.70).

11.5 't Hooft versus Veneziano limits

In QCD there are several species or flavors of quarks (u-, d-, s- and so on). We denote the number of flavors by N_f and associate a Greek letter α or β with a flavor index of the quark field.

The quark propagator then has the Kronecker delta-symbol with respect to the flavor indices in addition to Eq. (11.59):

$$\Big\langle \psi_i^\alpha \bar\psi_j^\beta \Big\rangle \;\;\propto\;\; \delta^{\alpha\beta}\delta_{ij}\,. \tag{11.74}$$

Their contraction results in

$$\sum_{\alpha=1}^{N_\mathrm{f}} \delta_{\alpha\alpha} \;=\; N_\mathrm{f}\,. \tag{11.75}$$

Therefore, an extra factor of N_f corresponds to each closed quark loop for the N_f flavors.

https://doi.org/10.1017/9781009402095.012 Published online by Cambridge University Press

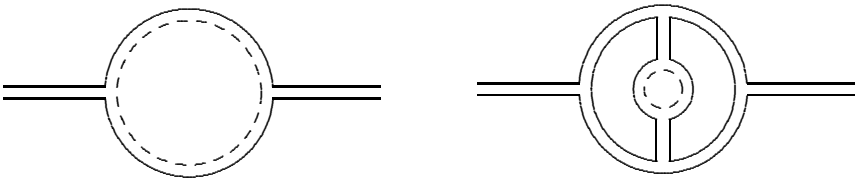

(a) (b)

Fig. 11.16. Diagrams with quark loops in the Veneziano limit. Color and flavor indices of a quark loop are represented by the solid and dashed single lines, respectively. Diagram (a) is $\sim g^2 N_\mathrm{f} \sim N_\mathrm{f}/N$. Diagram (b) is $\sim g^6 N^2 N_\mathrm{f} \sim N_\mathrm{f}/N$.

The limit when N_f is fixed as $N \to \infty$, as was considered in the original paper by 't Hooft [Hoo74a], is called the *'t Hooft limit*. Only valence quarks are left in the 't Hooft limit. Hence, it is associated with the quenched approximation which was discussed in the Remark on p. 158. In order for a meson to decay into other mesons built out of quarks, say for a ρ-meson to decay into a pair of π-mesons, a quark–antiquark pair must be produced out of the vacuum. Consequently, the ratios of meson widths to their masses are

$$\frac{\Gamma_\mathrm{total}}{M} \quad \sim \quad \frac{N_\mathrm{f}}{N} \tag{11.76}$$

in the 't Hooft limit. The ratio on the LHS of Eq. (11.76) is 10–15% experimentally for the ρ-meson. The hope of solving QCD in the 't Hooft limit is the hope to describe QCD with this accuracy.

An alternative large-N limit of QCD when $N_\mathrm{f} \sim N$ as $N \to \infty$ was proposed by Veneziano [Ven76]. Some diagrams for the gluon propagator, which involve one quark loop, are depicted in Fig. 11.16. The dashed single line represents propagation of the flavor index. Each closed loop of the dashed line is associated with the factor of N_f according to Eq. (11.75). This is analogous to the vector models which exactly describe the $O(N_\mathrm{f})$ flavor symmetry in this notation.

The diagrams in Fig. 11.16 contribute, respectively,

$$\text{Fig. 11.16a} \ \sim \ g^2 N_\mathrm{f} \ \sim \ \frac{N_\mathrm{f}}{N} \tag{11.77}$$

and

$$\text{Fig. 11.16b} \ \sim \ g^6 N^2 N_\mathrm{f} \ \sim \ \frac{N_\mathrm{f}}{N} \tag{11.78}$$

in the limit (11.13).

https://doi.org/10.1017/9781009402095.012 Published online by Cambridge University Press

Likewise, a more general diagram with L quark loops will contribute

$$L \text{ quark loops } \sim \left(\frac{N_{\rm f}}{N}\right)^L \left(\frac{1}{N^2}\right)^{\text{genus}} . \tag{11.79}$$

This formula obviously follows from Eq. (11.62) since each quark loop results in $N_{\rm f}$.

We see from Eq. (11.79) that quark loops are not suppressed at large N in the Veneziano limit

$$N_{\rm f} \sim N \to \infty \tag{11.80}$$

if the diagram is planar. Furthermore, the representation of a flavored quark by one solid and one dashed line is obviously similar to the double-line representation of a gluon. All that is said above concerning the topological expansion of pure gluodynamics holds for QCD with quarks in the Veneziano limit.

It is the Veneziano limit (11.80) that is related to the hadronic topological expansion in the dual-resonance models. In the Veneziano limit hadrons can have finite widths according to Eq. (11.76). I refer the reader to the original paper by Veneziano [Ven76] for further details.

There is an alternative way to show why virtual quarks are suppressed in the 't Hooft limit and survive in the Veneziano limit. Let us integrate over the quark fields which yields

$$\int \mathcal{D}\bar\psi\, \mathcal{D}\psi\, \mathrm{e}^{-\int \mathrm{d}^4x \left(\bar\psi\widehat\nabla\psi + m\bar\psi\psi\right)} = \mathrm{e}^{\mathrm{Tr}\ln\left(\widehat\nabla + m\right)} \tag{11.81}$$

as is discussed in Sect. 2.2. The trace in the exponent involves summation both over color and flavor indices, so that

$$\mathrm{Tr}\ln\left(\widehat\nabla + m\right) \sim N N_{\rm f} . \tag{11.82}$$

The order in N of the pure gluon action is $\mathcal{O}\left(N^2\right)$ as was discussed in the Remark on p. 232. Hence, the quark contribution to the action is $\sim N_{\rm f}/N$ in comparison with the gluon one. The quark determinant can be disregarded in the 't Hooft limit, but is essential in the Veneziano limit.

The consideration of the previous paragraph also explains why each quark loop contributes a factor of $\sim N_{\rm f}/N$. The exponent on the RHS of Eq. (11.81) is associated with one-loop diagrams. A diagram with L quark loops corresponds to the Lth term of the expansion of the exponential. This explains the factor of $(N_{\rm f}/N)^L$ in Eq. (11.79). A diagram with two quark loops, which appears in the second order of this expansion, is depicted in Fig. 11.17.

https://doi.org/10.1017/9781009402095.012 Published online by Cambridge University Press

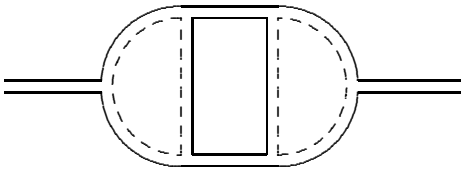

Fig. 11.17. Diagram with two quark loops in the Veneziano limit. The diagram is $\sim g^6 N N_{\rm f}^2 \sim (N_{\rm f}/N)^2$.

Remark on asymptotic freedom in the Veneziano limit

Though the number of flavors becomes large in the Veneziano limit, this does not mean that asymptotic freedom is lost. The leading-order coefficient of the $\mathcal{B}$-function of QCD with N colors and $N_{\rm f}$ flavors is given by

$$b = \frac{1}{4\pi^2}\left(-\frac{11}{3}N + \frac{2}{3}N_{\rm f}\right) \tag{11.83}$$

which reproduces Eq. (9.71) for $N = 3$. It is still negative if $N_{\rm f}/N < 11/2$ in the Veneziano limit.

Remark on phenomenology of multicolor QCD

While $N = 3$ in the real world, there are phenomenological indications that $1/N$ may be considered as a small parameter. We have already mentioned some of them in the text – the simplest one is that the ratio of the ρ-meson width to its mass, which is $\sim 1/N$, is small. Considering $1/N$ as a small parameter immediately leads to qualitative phenomenological consequences which are preserved by the planar diagrams associated with multicolor QCD, but are violated by the nonplanar diagrams.

The most important consequence is the relation of the $1/N$-expansion to the topological expansion in the dual-resonance model of hadrons. Vast numbers of properties of hadrons are explained by the dual-resonance model. A very clear physical picture behind this model is that hadrons are excitations of a string with quarks at the ends.

I shall briefly list some consequences of multicolor QCD.

(1) The "naive" quark model of hadrons emerges at $N = \infty$. Hadrons are built out of a pair of (valence or constituent) quark and antiquark $q\bar{q}$, while exotic states like $qq\bar{q}\bar{q}$ do not appear.

(2) The partial width of decay of the ϕ-meson, which is built out of $s\bar{s}$ (the strange quark and antiquark), into K^+K^- is $\sim 1/N$, while that

https://doi.org/10.1017/9781009402095.012 Published online by Cambridge University Press

into $\pi^+\pi^-\pi^0$ is $\sim 1/N^2$. This explains Zweig's rule. The masses of the ρ- and ω-mesons are degenerate at $N = \infty$.

(3) The coupling constant of the meson–meson interaction is small at large N.

(4) The widths of glueballs are $\sim 1/N^2$, i.e. they should be even narrower than mesons built out of quarks. The glueballs do not interact or mix with mesons at $N = \infty$.

All of these hadron properties (except the last one) agree approximately with experiment, and were well-known even before 1974 when multicolor QCD was introduced. Glueballs have not yet been detected experimentally (possibly because of their property listed in item (4)).

11.6 Large-N factorization

The vacuum expectation values of several colorless or white operators, which are singlets with respect to the gauge group, factorize in the large-N limit of QCD (or other matrix models). This property is similar to that already discussed in Sect. 10.5 for the vector models.

The simplest gauge-invariant operator in a pure $SU(N)$ gauge theory is the square of the non-Abelian field strength:

$$O(x) \;=\; \frac{1}{N^2}\,\mathrm{tr}\,F^2_{\mu\nu}(x)\,. \tag{11.84}$$

The normalizing factor provides the natural normalization

$$\left\langle \frac{1}{N^2}\,\mathrm{tr}\,F^2_{\mu\nu}(x) \right\rangle \;=\; \left\langle \frac{1}{N^2}\,F^a_{\mu\nu}(x)\,F^a_{\mu\nu}(x) \right\rangle \;\sim\; 1\,. \tag{11.85}$$

In order to verify the factorization in the large-N limit, let us consider the index-space diagrams for the average of two colorless operators $O(x_1)$ and $O(x_2)$, which are depicted in Fig. 11.18.

The graph in Fig. 11.18a represents the zeroth order of perturbation theory. It involves four closed index lines (the factor of N^4) and the normalization factor of $1/N^4$ according to the definition (11.84). Its contribution is

$$\text{Fig. 11.18a} \;\sim\; \frac{1}{N^2}N^2 \cdot \frac{1}{N^2}N^2 \;\sim\; 1\,, \tag{11.86}$$

i.e. $\mathcal{O}(1)$ in accord with the general estimate (11.85).

The graph in Fig. 11.18b involves a gluon line which is emitted and absorbed by the same operator $O(x_1)$. It has five closed index lines (the

https://doi.org/10.1017/9781009402095.012 Published online by Cambridge University Press

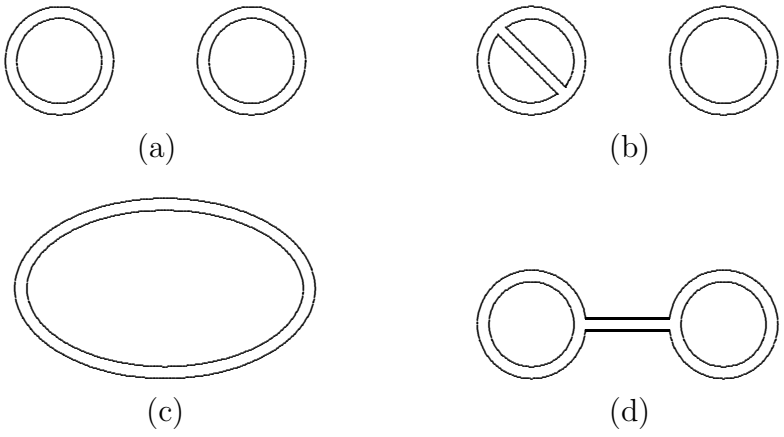

Fig. 11.18. Demonstration of the large-N factorization to the lowest orders of perturbation theory. The closed double line represents the average of the operator (11.84) to the zeroth order in g. Diagrams (a) and (b), which are associated with the factorized part of the average on the LHS of Eq. (11.90), are $\mathcal{O}(1)$. Diagrams (c) and (d), which would violate the factorization, are suppressed by $1/N^2$.

factor of N^5), the normalization factor of $1/N^4$, and g^2 owing to two three-gluon vertices. Its contribution is

$$\text{Fig. 11.18b} \;\sim\; g^2 N \;\sim\; 1\,, \tag{11.87}$$

i.e. also $\mathcal{O}(1)$ in the limit (11.13).

The graph in Fig. 11.18c is of the same type as the graph in Fig. 11.18a, but the double lines now connect two different operators. It has two closed index lines (the factor of N^2) and the normalization factor of $1/N^4$, so that its contribution

$$\text{Fig. 11.18c} \;\sim\; \frac{1}{N^2} \tag{11.88}$$

is suppressed by $1/N^2$.

The graph in Fig. 11.18d, which is of the same order in the coupling constant as the graph in Fig. 11.18b, involves only three closed index lines (the factor of N^3) and is of order $1/N^2$:

$$\text{Fig. 11.18d} \;\sim\; g^2 \frac{1}{N} \;\sim\; \frac{1}{N^2}\,. \tag{11.89}$$

Therefore, it is suppressed by $1/N^2$ in the large-N limit. For this graph, the gluon line is emitted and absorbed by different operators $O(x_1)$ and $O(x_2)$.

https://doi.org/10.1017/9781009402095.012 Published online by Cambridge University Press

This lowest-order example illustrates the general property that only (planar) diagrams with gluon lines emitted and absorbed by the same operators survive as $N \to \infty$. Hence, correlations between the colorless operators $O(x_1)$ and $O(x_2)$ are of order $1/N^2$, so that the *factorization* property holds as $N \to \infty$:

$$\left\langle \frac{1}{N^2} \operatorname{tr} F^2(x_1) \frac{1}{N^2} \operatorname{tr} F^2(x_2) \right\rangle = \left\langle \frac{1}{N^2} \operatorname{tr} F^2(x_1) \right\rangle \left\langle \frac{1}{N^2} \operatorname{tr} F^2(x_2) \right\rangle + \mathcal{O}\big(N^{-2}\big) . \tag{11.90}$$

For a general set of gauge-invariant operators $O_1, \ldots, O_n$, the factorization property can be represented by

$$\langle\, O_1 \cdots O_n \,\rangle = \langle\, O_1 \,\rangle \cdots \langle\, O_n \,\rangle + \mathcal{O}\big(N^{-2}\big) . \tag{11.91}$$

This is analogous to Eq. (10.123) for the vector models.

The factorization in large-N QCD was first discovered by A.A. Migdal in the late 1970s. The important observation that the factorization implies a semiclassical nature of the large-N limit of QCD was made by Witten [Wit79]. We shall discuss this in the next two sections.

The factorization property also holds for gauge-invariant operators constructed from quarks as in Eq. (11.63). For the case of several flavors $N_{\rm f}$, we normalize these quark operators by

$$O_\Gamma = \frac{1}{N_{\rm f} N} \bar\psi \Gamma \psi . \tag{11.92}$$

Here Γ denotes one of the combination of the γ-matrices:

$$\Gamma = \mathbb{I},\ \gamma_5,\ \gamma_\mu,\ \mathrm{i}\gamma_\mu\gamma_5,\ \Sigma_{\mu\nu} = \frac{1}{2\mathrm{i}}[\gamma_\mu, \gamma_\nu] \,, \ldots . \tag{11.93}$$

The lowest-order diagrams of perturbation theory for the average of two quark operators (11.92) are depicted in Fig. 11.19. The estimation of their order in $1/N$ is analogous to that for the pure gluon graphs in Fig. 11.18.

The graph in Fig. 11.19a represents the zeroth order of perturbation theory for the average of two quark operators. It involves two closed color and two closed flavor index lines (the factor of $N_{\rm f}^2 N^2$) and the normalization factor of $1/(N_{\rm f} N)^2$ according to the definition (11.92). Its contribution is

$$\text{Fig. 11.19a} \ \sim\ \frac{1}{N_{\rm f}^2 N^2} N_{\rm f}^2 N^2 \ \sim\ 1 . \tag{11.94}$$

This justifies the normalization factor in Eq. (11.92).

https://doi.org/10.1017/9781009402095.012 Published online by Cambridge University Press

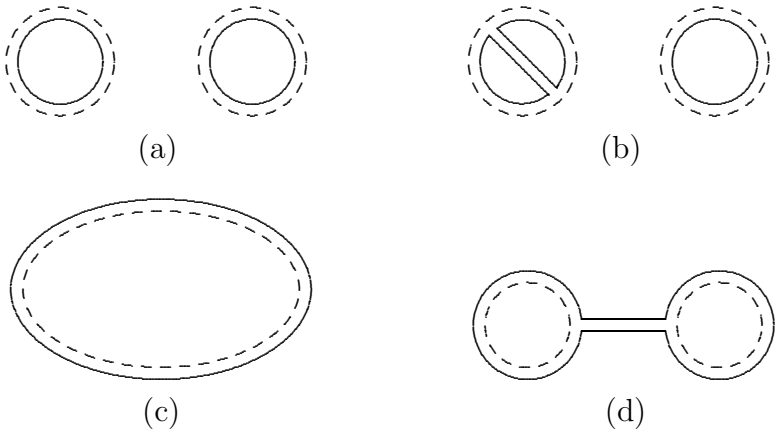

Fig. 11.19. Same as in Fig. 11.18 but for quark operators (11.92). The solid and dashed lines are associated with color and flavor indices, respectively. Diagrams (a) and (b), which contribute to the factorized part of the average on the LHS of Eq. (11.98), are $\mathcal{O}(1)$. Diagrams (c) and (d), which would violate the factorization, are suppressed by $1/(N_{\rm f}N)$ and $1/N^2$, respectively.

The graph in Fig. 11.19b involves a gluon line which is emitted and absorbed by the same quark operator. It has three closed color and two closed flavor index lines (the factor of $N_{\rm f}^2N^3$), the normalization factor of $1/(N_{\rm f}N)^2$, and g^2 arising from two quark–gluon vertices. Its contribution is

$$\text{Fig. 11.19b} \;\sim\; \frac{1}{N_{\rm f}^2N^2}N_{\rm f}^2g^2N^3 \;\sim\; g^2N \;\sim\; 1 \tag{11.95}$$

in full analogy with the pure gluon diagram in Fig. 11.18b.

The graph in Fig. 11.19c is similar to the graph in Fig. 11.18c – the lines connect two different quark operators. It has one closed color and one closed flavor index lines (the factor of $N_{\rm f}N$) and the normalization factor of $1/(N_{\rm f}N)^2$, so that its contribution

$$\text{Fig. 11.19c} \;\sim\; \frac{1}{N_{\rm f}N} \tag{11.96}$$

is suppressed by $1/(N_{\rm f}N)$.

Finally, the graph in Fig. 11.19d involves a gluon line which is emitted by one quark operator and absorbed by the other. It has one closed color and two closed flavor index lines (factor of $N_{\rm f}^2N$), the normalization factor of $1/(N_{\rm f}N)^2$, and g^2 owing to two quark–gluon vertices. Its contribution

$$\text{Fig. 11.19d} \;\sim\; \frac{1}{N_{\rm f}^2N^2}N_{\rm f}^2g^2N \;\sim\; \frac{g^2}{N} \;\sim\; \frac{1}{N^2} \tag{11.97}$$

is suppressed by $1/N^2$ in the limit (11.13).

https://doi.org/10.1017/9781009402095.012 Published online by Cambridge University Press

We see that the factorization of the gauge-invariant quark operators holds both in the 't Hooft and Veneziano limits:

$$\langle O_{\Gamma_1} \cdots O_{\Gamma_n} \rangle \;=\; \langle O_{\Gamma_1} \rangle \cdots \langle O_{\Gamma_n} \rangle + \mathcal{O}(1/(N_{\rm f}N)) \,. \qquad (11.98)$$

The nonfactorized part, which is associated with connected diagrams, is $\sim 1/N$ in the 't Hooft limit. This leads, in particular, to the coupling constant of meson–meson interaction of order $1/N$, clarifying the property of multicolor QCD listed in item (3) on p. 237. The Veneziano limit is analogous to pure gluodynamics as has already been mentioned.

It is worth noting that the factorization can be seen alternatively (at all orders of perturbation theory) from Eq. (11.70) for the contribution of a generic connected graph of genus h with B external boundaries which are precisely associated with the quark operators O_Γ, as is explained in Sect. 11.4. The diagrams with gluon lines emitted and absorbed by the same operator as in Fig. 11.19b are products of diagrams having only one boundary. Hence, their contribution is of order one. Otherwise, the diagrams with gluon lines emitted and absorbed by two different operators as in Fig. 11.19d have two boundaries. According to Eq. (11.70), their contribution is suppressed by $1/N^2$. Alternatively, the diagrams as in Fig. 11.19c (including its planar dressing by gluons) have one boundary.* Their contribution is $\mathcal{O}(1)$ times $1/(N_{\rm f}N)$ coming from the normalization of the operator (11.92). This proves the factorization property (11.98) at all orders of perturbation theory.

Remark on factorization beyond perturbation theory

The large-N factorization can also be verified at all orders of the strong-coupling expansion in the $SU(N)$ lattice gauge theory. A nonperturbative proof of the factorization will be given in the next chapter using quantum equations of motion (the loop equations).

Problem 11.7 Prove the factorization of the Wilson loop operators within the strong-coupling expansion of the $SU(N)$ lattice gauge theory as $N \to \infty$.

Solution Let us first estimate the order in N of the Wilson loop average (6.42). The explicit result to the leading order in β is given by Eqs. (6.73) and (6.72), where

$$\beta \;\sim\; N^2 \qquad (11.99)$$

in the limit (11.13) as prescribed by Eq. (6.32). Therefore, $W(C) \sim 1$ in the large-N limit.

* In the dual-resonance model, they are associated with the meson–meson interaction arising from an exchange of constituent quarks.

https://doi.org/10.1017/9781009402095.012 Published online by Cambridge University Press

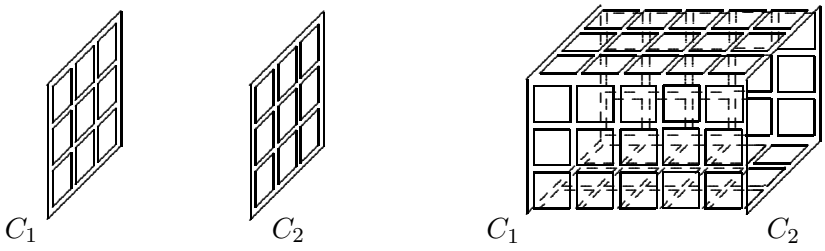

Fig. 11.20. Factorization of the Wilson loop operators in the strong-coupling expansion as $N \to \infty$. The surfaces are constructed from plaquettes which come from the expansion of the exponential of the lattice action. Each link in the surface is passed at least twice: otherwise the result vanishes. Diagram (a) involves two separate surfaces enclosed by Wilson loops. It contributes to the factorized part of the average on the LHS of Eq. (11.101). The surface in diagram (b) connects two different Wilson loops and would violate factorization. It has two boundaries and its contribution is suppressed by $1/N^2$ according to the general formula (11.100).

To be precise, we first perform the strong-coupling expansion in β and then set $N \to \infty$ in each term of the strong coupling expansion. As we shall see in a moment, the actual parameter is β/N^2, so that the limits $\beta \to 0$ and $N \to \infty$ are interchangeable.

It is easy to estimate the order in N of any graph of the strong coupling expansion for $W(C)$, which looks like that in Fig. 6.8 on p. 116. Let the plaquettes fill an arbitrary surface enclosed by the loop C, with n_2, n_1, and n_0 being the number of plaquettes, links, and sites which belong to the surface. Each plaquette contributes β/N since it comes from the expansion of the exponential of the lattice action, each link contributes $1/N$ owing to Eq. (6.60), and each site contributes N since it is associated with summing over the color indices owing to Eq. (6.70). Accounting for the normalization factor of $1/N^B$, where $B = 1$ is the number of boundaries, the contribution is of order

$$\left(\frac{\beta}{N}\right)^{n_2} N^{-n_1+n_0-B} \sim \left(\frac{\beta}{N^2}\right)^{n_2} N^{n_2-n_1+n_0-B} \sim \left(\frac{\beta}{N^2}\right)^{n_2} \left(\frac{1}{N}\right)^{2h+2(B-1)}, \tag{11.100}$$

where we have used Euler's theorem (11.68). In the limit (11.99), the contribution does not depend on the order of the strong-coupling expansion and is completely determined by the number B of boundaries and the genus h of the surface. This is analogous to the perturbation theory. For the minimal surface, we reproduce previous results.

We are now in a position to analyze the order in N of different terms in the strong-coupling expansion of the average of two Wilson loop operators. The factorized part results from the surfaces of the type depicted in Fig. 11.20a, which are spanned by each individual loop. Its contribution is $\mathcal{O}(1)$ as $N \to \infty$. A nonfactorized part emerges from surfaces of the type depicted in Fig. 11.20b,

https://doi.org/10.1017/9781009402095.012 Published online by Cambridge University Press

which connect two different Wilson loops. They look like a cylinder and have two boundaries. Their contribution is suppressed by $1/N^2$ according to the general formula (11.100).

Thus, we have proven the factorization property

$$\left\langle \frac{1}{N}\mathrm{tr}\, U(C_1)\, \frac{1}{N}\mathrm{tr}\, U(C_2) \right\rangle \;=\; \left\langle \frac{1}{N}\mathrm{tr}\, U(C_1) \right\rangle \left\langle \frac{1}{N}\mathrm{tr}\, U(C_2) \right\rangle + \mathcal{O}\big(N^{-2}\big) \tag{11.101}$$

at all orders of the strong-coupling expansion.

Problem 11.8 Find the relation between the Wilson loop averages in the fundamental and adjoint representations for an $SU(N)$ pure gauge theory at large N.

Solution The characters in the fundamental and adjoint representations are related by Eq. (6.28). Using the factorization formula (11.101) with coinciding contours C_1 and C_2, we obtain

$$W_{\mathrm{adj}}(C) \;=\; \big[W_{\mathrm{fun}}(C)\big]^2 + \mathcal{O}\big(N^{-2}\big)\,. \tag{11.102}$$

As was discussed in Part 2, the Wilson loop average in the fundamental representation obeys the area law (6.75). The same is true at $N = \infty$ for the Wilson loop average in the adjoint representation owing to Eq. (11.102). In particular, the string tensions in the fundamental and adjoint representations at $N = \infty$ are related by

$$K_{\mathrm{adj}} \;=\; 2K_{\mathrm{fun}}\,. \tag{11.103}$$

On the other hand, the adjoint test quark can be screened at finite N by a gluon produced out of the vacuum. This is similar to the breaking of the flux tube in the fundamental representation by a quark–antiquark pair, which is discussed in Sect. 9.5. Therefore, the perimeter law (6.79) must dominate for large contours. The point is that the perimeter law appears owing to connected diagrams which are suppressed as $1/N^2$:

$$W_{\mathrm{adj}}(C) \quad \stackrel{\text{large } C}{\longrightarrow} \quad \mathrm{e}^{-2KA_{\min}(C)} + \frac{1}{N^2}\,\mathrm{e}^{-\mu\cdot L(C)}. \tag{11.104}$$

These properties of the adjoint representation were first pointed out in [KM81].

11.7 The master field

The large-N factorization in QCD assumes that gauge-invariant objects behave as c-numbers, rather than as operators. Likewise for vector models, this suggests that the path integral is dominated by a saddle point.

We have already seen in Sect. 10.5 that the factorization in the vector models does not mean that the fundamental field itself, for instance $\vec{n}$ in the sigma-model, becomes "classical". It is the case, instead, for a singlet composite field.

https://doi.org/10.1017/9781009402095.012 Published online by Cambridge University Press

We are now going to apply a similar idea to the Yang–Mills theory, the partition function of which is

$$Z \;=\; \int \mathcal{D}A^a_\mu \, \mathrm{e}^{-\int \mathrm{d}^4x \, \frac{1}{4} F^a_{\mu\nu} F^a_{\mu\nu}} \,. \tag{11.105}$$

The action, $\sim N^2$, is large as $N \to \infty$, but the entropy is also $\sim N^2$ as a result of the $N^2 - 1$ integrations over A^a_μ:

$$\mathcal{D}A^a_\mu \;\sim\; \mathrm{e}^{N^2} . \tag{11.106}$$

Consequently, the saddle-point equation of the large-N Yang–Mills theory is *not* the classical one which is given by*

$$\frac{\delta S}{\delta A^a_\nu} \;=\; -\,(\nabla_\mu F_{\mu\nu})^a \;=\; 0\,. \tag{11.107}$$

The idea is to rewrite the path integral over A_μ for the Yang–Mills theory as that over a colorless composite field $\Phi[A]$, likewise this was done in Sect. 10.4 for the sigma-model. The expected new path-integral representation of the partition function (11.105) would be something like

$$Z \;\propto\; \int \mathcal{D}\Phi \, \frac{1}{\left| \frac{\partial \Phi[A]}{\partial A^a_\mu} \right|} \, \mathrm{e}^{-N^2 S[\Phi]} \,. \tag{11.108}$$

The Jacobian

$$\left| \frac{\partial \Phi[A]}{\partial A^a_\mu} \right| \;\equiv\; \mathrm{e}^{-N^2 J[\Phi]} \tag{11.109}$$

in Eq. (11.108) is related to the old entropy factor, so that $J\,[\Phi] \sim 1$ in the large-N limit.

The original partition function (11.105) can be then rewritten as

$$Z \;\propto\; \int \mathcal{D}\Phi \, \mathrm{e}^{N^2 J[\Phi] - N^2 S[\Phi]}, \tag{11.110}$$

where $S[\Phi]$ represents the Yang–Mills action in the new variables. The new entropy factor of $\mathcal{D}\Phi$ is $\mathcal{O}(1)$ because the variable $\Phi[A]$ is a color singlet. The large parameter N enters Eq. (11.110) only in the exponent. Therefore, the saddle-point equation can be immediately written as

$$\frac{\delta S}{\delta \Phi} \;=\; \frac{\delta J}{\delta \Phi} \,. \tag{11.111}$$

* It was already discussed in Problem 5.1 on p. 87.

https://doi.org/10.1017/9781009402095.012 Published online by Cambridge University Press

Remembering that Φ is a functional of A_μ, $\Phi \equiv \Phi[A]$, we rewrite the saddle-point equation (11.111) as

$$\frac{\delta S}{\delta A^a_\nu} \;=\; -\,(\nabla_\mu F_{\mu\nu})^a \;=\; \frac{\delta J}{\delta A^a_\nu}\,. \tag{11.112}$$

It differs from the classical Yang–Mills equation (11.107) by the term on the RHS coming from the Jacobian (11.109).

Given $J[\Phi]$, which depends on the precise from of the variable $\Phi[A]$, Eq. (11.112) has a solution

$$A_\mu(x) \;=\; A^{\rm cl}_\mu(x)\,. \tag{11.113}$$

Let us first assume that there exists only one solution to Eq. (11.112). Then the path integral is saturated by a single configuration (11.113), so that the vacuum expectation values of gauge-invariant operators are given by their values at this configuration:

$$\langle\, O\,\rangle \;=\; O\Big(A^{\rm cl}_\mu(x)\Big)\,. \tag{11.114}$$

The factorization property (11.91) will obviously be satisfied.

The existence of such a classical field configuration in multicolor QCD was conjectured by Witten [Wit79]. It was discussed in the lectures by Coleman [Col79] who called it the *master field*. Equation (11.112) which determines the master field is often referred to as the master-field equation.

A subtle point with the master field is that a solution to Eq. (11.112) is determined only up to a gauge transformation. To preserve gauge invariance, it is more reasonable to speak about the whole gauge orbit as a solution of Eq. (11.112). However, this will not change Eq. (11.114) since the operator O is gauge invariant.

The conjecture concerning the existence of the master field has surprisingly rich consequences. Since vacuum expectation values are Poincaré invariant, the RHS of Eq. (11.114) is also. This implies that $A^{\rm cl}_\mu(x)$ must itself be Poincaré invariant up to a gauge transformation: a change of $A^{\rm cl}_\mu(x)$ under translations or rotations can be compensated by a gauge transformation. Moreover, there must exist a gauge in which $A^{\rm cl}_\mu(x)$ is space-time-independent: $A^{\rm cl}_\mu(x) = A^{\rm cl}_\mu(0)$. In this gauge, rotations must be equivalent to a global gauge transformation, so that $A^{\rm cl}_\mu(0)$ transforms as a Lorentz vector.

In fact, the idea concerning such a master field in multicolor QCD may not be correct as was pointed out by Haan [Haa81]. The conjecture concerning the existence of only one solution to the master-field equation (11.112) seems to be too strong. If several solutions exist, one needs

https://doi.org/10.1017/9781009402095.012 Published online by Cambridge University Press

an additional averaging over these solutions. This is a very delicate matter, since this additional averaging must still preserve the factorization property. One might be better to think about this situation as if $A_\mu^{\rm cl}(0)$ were an operator in some Hilbert space rather than a c-valued function. This is simply because $A_\mu^{\rm cl}(0)$ is, in the matrix notation (11.1), an $N \times N$ matrix which becomes, as $N \to \infty$, an infinite matrix, or an operator in Hilbert space. Such an operator-valued master field is sometimes called the master field in the *weak* sense, while the above conjecture concerning a single classical configuration of the gauge field, which saturates the path integral, is called the master field in the *strong* sense.

The concept of the master field is rather vague until a precise form of the composite field $\Phi[A]$, and consequently the Jacobian $\Phi[A]$ that enters Eq. (11.112), is defined. However, what is important is that the master field (in the weak sense) is space-time-independent. This looks like a simplification of the problem of solving large-N QCD. A Hilbert space, in which the operator $A_\mu^{\rm cl}(0)$ acts, should be specified by $\Phi[A]$. In the next section we shall consider a realization of these ideas for the case of $\Phi[A]$ given by the trace of the non-Abelian phase factor for closed contours.

Remark on noncommutative probability theory

An adequate mathematical language for describing the master field in multicolor QCD (and, generically, in matrix models at large N) was found by I. Singer in 1994. It is based on the concept of free random variables of noncommutative probability theory, introduced by Voiculescu [VDN95]. How to describe the master field in this language and some other applications of noncommutative free random variables to the problems of planar quantum field theory are discussed in [Dou95, GG95].

11.8 $1/N$ as semiclassical expansion

A natural candidate for the composite operator $\Phi[A]$ from the previous section is given by the trace of the non-Abelian phase factor for closed contours – the Wilson loop. It is labeled by the loop C in the same sense as the field $A_\mu(x)$ is labeled by the point x, so we shall use the notation

$$\Phi(C) \equiv \Phi[A] = \frac{1}{N} \operatorname{tr} \boldsymbol{P}\, \mathrm{e}^{\mathrm{i}g \oint_C \mathrm{d}x^\mu A_\mu(x)}. \tag{11.115}$$

Nobody up to now has managed to reformulate QCD at finite N in terms of $\Phi(C)$ in the language of the path integral. This is due to the fact that self-intersecting loops are not independent (they are related by the so-called Mandelstam relations [Man79]),* and the Jacobian is huge.

* See, for example, Appendix C of the review [Mig83].

https://doi.org/10.1017/9781009402095.012 Published online by Cambridge University Press

The reformulation was performed [MM79] in the language of Schwinger–Dyson or loop equations which will be described in the next chapter.

Schwinger–Dyson equations are a convenient way of performing the semiclassical expansion, which is an alternative to the path integral. Let us illustrate an idea of how to do this by an example of the φ^3 theory, the Schwinger–Dyson equations of which are given by Eq. (2.47).

The RHS of Eq. (2.47) is proportional to Planck's constant $\hbar$ as is explained in Sect. 2.5. In the semiclassical limit $\hbar \to 0$, we obtain

$$\left(-\partial_1^2 + m^2\right) \langle \varphi(x_1) \cdots \varphi(x_n) \rangle + \frac{\lambda}{2} \left\langle \varphi^2(x_1) \cdots \varphi(x_n) \right\rangle \quad = \quad 0\,, \qquad (11.116)$$

the solution of which is of the factorized form

$$\langle \varphi(x_1) \cdots \varphi(x_n) \rangle \quad = \quad \langle \varphi(x_1) \rangle \cdots \langle \varphi(x_n) \rangle + \mathcal{O}(\hbar) \qquad (11.117)$$

provided that

$$\langle \varphi(x) \rangle \quad \equiv \quad \varphi_{\rm cl}(x) \qquad (11.118)$$

obeys

$$\left(-\partial^2 + m^2\right) \varphi_{\rm cl}(x) + \frac{\lambda}{2} \varphi_{\rm cl}^2(x) \quad = \quad 0\,. \qquad (11.119)$$

Equation (11.119) is nothing but the classical equation of motion for the φ^3 theory, which specifies extrema of the action (2.22) entering the path integral (2.2). Thus, we have reproduced, using the Schwinger–Dyson equations, the well-known fact that the path integral is dominated by a classical trajectory as $\hbar \to 0$. It is also clear how to perform the semiclassical expansion in $\hbar$ in the language of the Schwinger–Dyson equations: one should solve Eq. (2.47) by iteration.

The reformulation of multicolor QCD in terms of the loop functionals $\Phi(C)$ is, in a sense, a realization of the idea of the master field in the weak sense, when the master field acts as an operator in the space of loops. The loop equation of the next chapter will be a sort of master-field equation in the loop space.

Remark on the large-N limit as statistical averaging

There is yet another, purely statistical, explanation why the large-N limit is a "semiclassical" limit for the collective variables $\Phi(C)$. The matrix $U^{ij}[C_{xx}]$, that describes the parallel transport along a closed contour C_{xx}, can be reduced by the unitary transformation to

$$U[C_{xx}] \quad = \quad \Omega[C_{xx}]\, {\rm diag} \left({\rm e}^{{\rm i}g\alpha_1(C)}, \ldots, {\rm e}^{{\rm i}g\alpha_N(C)} \right) \Omega^\dagger[C_{xx}]\,. \qquad (11.120)$$

https://doi.org/10.1017/9781009402095.012 Published online by Cambridge University Press

Then $\Phi(C)$ is given by

$$\Phi(C) \;=\; \frac{1}{N}\sum_{j=1}^{N} \mathrm{e}^{\mathrm{i}g\alpha_j(C)}. \tag{11.121}$$

The phases $\alpha_j(C)$ are gauge invariant modulo permutations and normalized so that $\alpha_j(C) \sim 1$ as $N \to \infty$. For simplicity we omit below all the indices (including space ones) except for color.

The commutator of Φs can be estimated using the representation (11.121). Since

$$\big[\alpha_i(C),\, \alpha_j(C')\big] \;\propto\; \delta_{ij}\,, \tag{11.122}$$

one obtains

$$\big[\Phi(C)\,,\, \Phi(C')\big] \;\sim\; g^2\frac{1}{N} \;\sim\; \frac{1}{N^2} \tag{11.123}$$

in the limit (11.13), i.e. the commutator can be neglected as $N \to \infty$, and the field $\Phi(C)$ becomes classical.

Note that the commutator (11.123) is of order $1/N^2$. One factor of $1/N$ is because of g in the definition (11.121) of $\Phi(C)$, while the other has a deeper reason. Let us image the summation over j in Eq. (11.121) as some statistical averaging. It is well-known in statistics that such averages fluctuate weakly as $N \to \infty$, so that the dispersion is of order $1/N$. It is this factor that emerges in the commutator (11.123).

The factorization is valid only for the gauge-invariant quantities which involve the averaging over the color indices, such as that in Eq. (11.121). There is no reason to expect factorization for gauge invariants which do not involve this averaging and therefore fluctuate strongly even at $N = \infty$. An explicit example of such strongly fluctuating gauge-invariant quantities was first constructed in [Haa81].

This Remark may be summarized to give that the factorization arises from the additional statistical averaging in the large-N limit. There is no reason to assume the existence of a master field in the strong sense in order to explain the factorization.

https://doi.org/10.1017/9781009402095.012 Published online by Cambridge University Press